Chiral Selectivity of Porphyrin-ZnO Nanoparticles Conjugates

Manuela Stefanelli,[‡, §] Gabriele Magna,[†,§] Francesca Zurlo,[‡] M. Federica Caso,[ǂ] Elisabetta Di Bartolomeo,[‡] Simonetta Antonaroli,[‡] Mariano Venanzi,[‡] Roberto Paolesse,*[,‡] Corrado Di Natale,*[, †] and Donato Monti*[,‡]

[‡] Department of Chemical Science and Technology, University of Rome Tor Vergata, Via della Ricerca Scientifica, 00133 Rome, Italy

[†] Department of Electronic Engineering, University of Rome Tor Vergata, Via del Politecnico 1, 00133 Rome, Italy

[ǂ] Italian National Agency for New Technologies, Energy and Sustainable Economic Development (ENEA), Casaccia Research Centre, Via Anguillarese 301, 00123 Rome, Italy

Corresponding Authors

*monti@stc.uniroma2.it; ORCID 0000-0002-6166-8536

roberto.paolesse@uniroma2.it; ORCID 0000-0002-2380-1404

dinatale@ing.uniroma2.it; ORCID 0000-0002-0543-4348

Author Contributions

All authors have given approval to the final version of the manuscript.

§These authors contributed equally. Manuela Stefanelli ORCID 0000-0001-8563-8043, Magna Gabriele ORCID 0000-0003-2140-0110, Maria Federica Caso ORCID 0000-0002-9723-5265

Keywords: porphyrin, ZnO nanoparticles, supramolecular chirality, chiral surface, hybrid materials, chiral sensing, quartz microbalances

ABSTRACT:

The recognition of enantiomers is one of the most arduous challenge for chemical sensors development. Although several chiral systems have been developed so far, their effective exploitation as sensitive layer in chemical sensors is complicated by several practical implications that hinder the stereoselective recognition in solid-state. In this paper we show how preparing chiral solid films by

using a hybrid material approach where chiral porphyrin derivatives are grafted onto zinc oxide nanoparticles. Circular Dichroism evidences that solid-state film retains supramolecular chirality due to porphyrin interactions and presents an additional CD feature in correspondence to the absorbance of ZnO (375 nm), suggesting the induction of chirality in the underneath zinc oxide nanoparticles. The capability of hybrid material to detect and recognize vapours of enantiomer pairs has been evaluated fabricating gas sensors based on quartz microbalances. Chiral films of porphyrin as itself are used for comparison. The sensor based on functionalized nanostructures presented a remarkable stereoselectivity in the recognition of limonene enantiomers, whose features to intercalate in the porphyrin layers make this terpene an optimal chiral probe. Chiroptical and stereoselective properties of hybrid material confirm that porphyrin capped ZnO nanostructures is a viable procedure for the formation of chiral selective surfaces.

INTRODUCTION

Chirality has increasingly nurtured scientific interests because, beyond the concepts related with the foundation of Life, it has remarkable implications in practical fields dealing with chemistry, biology and medicine. The development of chiral materials, coupled with nanotechnology, constitutes a deeply pursued target, having a wide range of exploitation in many unique areas as catalysis,[1] nonlinear optics,[2] materials science[3] and sensors.[4]

The design of chiral molecules requires versatile and easily tuneable molecular elements. To this regard, porphyrins are unparalleled by any other systems and then they have been diffusely used as building blocks to assemble organized materials expressing elements of chirality at supramolecular level.[5] For example it has been illustrated that supramolecular assemblies of porphyrin derivatives bearing an appended (L)-proline functionality on a meso phenyl position exhibit strong chiroptical activity when aggregating in hydroalcoholic solution.[6] Generally, such chiral features are difficult to be transferred in solid state film, due to the influence of outside factors like the hydrophilic/hydrophobic properties of substrates or the process of solvent evaporation. Indeed, the possibility to fabricate solid film possessing chiral activity is surely attractive for the development of stereoselective gas sensors, a field far less explored than the enantiomer discrimination in solutions. The control of chiral compounds is becoming an important task in different fields, because chiral molecules are conventionally used and produced by pharmaceutical, food, agrochemical, perfume, and cosmetics industries, and consequently they are released into the environment.[7] However the chiral nature of waste is generally not considered in detail, whilst the environmental impact of refuse strongly depends on the chirality because the interactions of enantiomers with the biological

ecosystem, such as their uptake, metabolism and excretion, are stereoselective and the physiological activity of the enantiomers differs significantly.

In this context, chemical sensors can represent a suitable solution for a fast, simple and real-time analysis for recognizing and discriminating chiral molecules in situ. However**,** to develop reliable sensors is necessary to define chiral receptors able to discriminate in the solid phase enantiomers via specific interactions. This is a challenging task and for this reason only sparse examples of gas sensors able to feature chiral discrimination have been reported in the literature.[8]

A simple method to produce chiral films consists in immobilizing molecules into monolayers to preserve the chiral information stored by the monomers as well as to offer easily available chiral centres to volatile compounds. However, this molecular displacement produces only a limited amount of adsorption sites located at the surface. Accordingly, we reported that in case of quartz microbalances coated with monolayers of Co porphyrin dyads functionalized with a chiral dithiane group, the stereoselectivity can be only observed at very low concentrations.[9] In this context, the possibility to increase the surface area of sensing layers could greatly extend the range of detection of volatile species. However, the gas selectivity of thick films depends on factors additional to the ones that can be found in a monolayer arrangement, including either the film stability and porosity, the analyte diffusion or the unavailability of the chiral sites.

We recently studied, in fact, the formation of chiral supramolecular structures formed by cationic chiral porphyrin derivatives (**MPL(+)**; see SI, Chart S1 and Figure S1).[6b-c] Although the chirality of these structures was preserved after the deposition onto inorganic substrates,[10] the expected stereoselective properties were not found after the film deposition onto the surface of quartz microbalance and the exposure to vapours of chiral analytes (unpublished results, see Figure S1 in SI and results section below).

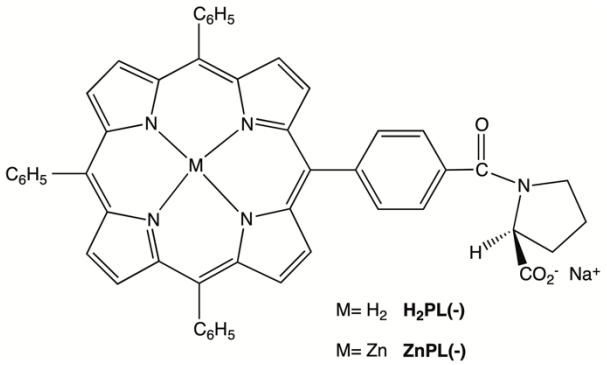

Chart 1. Molecular structures of the porphyrin derivatives investigated in this paper.

A compromise between the arrangement in monolayers and supramolecular self-assemblies may be represented by hybrid materials where, for example, a very thin layer of receptor molecules can be

grafted onto inorganic nanostructures and then deposited onto the sensor surface to produce a solid film. In this way, the thickness of organic film is delineated during the first step when nanostructures are functionalized. Thereafter, the hybrid material can be deposited virtually *ad libitum* onto sensor surfaces without affecting the amount of porphyrin layered onto the single nanoparticles. At last, the empty regions and spaces between the clusters of nanoparticles are easily accessible to volatile compounds, preventing the undesirable concentration range limitation found in monolayers. The advantages of this kind of hybrid material have been already demonstrated in chemical sensors and this concept is here applied in the case ZnO nanoparticles (**ZnONP**) functionalized with the **ZnPL(-)** derivative through the aminoacidic carboxylic group grafting the macrocycle at the oxide surface (Chart1). ZnO properties are well known and they are exploited in many diverse applications such as catalysis, gas sensors, and organic solar cells.[11] Furthermore, ZnO is prone to form heterogeneous structures with organic and inorganic materials, including, *inter alia*, porphyrin capped nanostructures.[12] Sensing properties of such hybrid materials have been extensively studied and the results show that the molecular arrangement of porphyrins onto the ZnO surface greatly influences the sensor sensitivity and selectivity.[13]

For sake of comparison, **ZnPL(-)** has been also used as itself to produce solid films starting from both aggregative and non-aggregative conditions in solution (*vide infra*). Similarly to other proline-functionalized porphyrin derivatives,[6] **ZnPL(-)** has the aptitude to form chiral aggregates in ethanol-water solution thanks to the hydrophobic effect, whereas monomeric state of **ZnPL(-)** can be simply obtained in absolute ethanol solution. The three materials have been extensively characterized with particular attention to their chiroptical properties, both in solution and in the solid state. The stereoselectivity of these systems towards enantiomer vapours of limonene, alpha-pinene and butan-2-ol has been studied, layering the materials on quartz microbalances (QMBs). QMBs provide both a quantitative measure of the total amounts of adsorbed analytes and the relative magnitude of stereoselective interactions respect to the overall ones, which mostly rely, in the case study, on non-specific London dispersion forces and $\pi-\pi$ interactions.

CD analysis reveals that layered films of Zn porphyrin-ZnO nanoparticles (named **ZnPL(-)-ZnONP** hereafter) retain the chiroptical properties of the macrocycles, displaying stereoselectivity thanks to the interparticle supramolecular interactions. These aspects represent promising features for the development of reliable and efficient sensors based on the implementation of large chiral surfaces.

2. EXPERIMENTAL SECTION

Materials and methods. Reagents and solvents were purchased from either Sigma Aldrich, Merck, or Carlo Erba and were used as received. (R)-(+)-limonene (97% purity) and (S)-(-)-limonene (96%

purity), (R)-(−)-Butan-2-ol (purity 99%), (S)-(+)-Butan-2-ol (purity 99%), (+)-alpha-pinene (purity >99%), (-)-alpha-pinene (purity >99%) were commercially available from Sigma Aldrich.

Thin-layer chromatography (TLC) was performed on Merck silica gel plates. Chromatographic purification on column was accomplished by using silica gel 60 (70–230 mesh, Sigma Aldrich) as the stationary phase. ^{1}H NMR spectrum of the novel porphyrin derivative **ZnPL(-)** is recorded with a Bruker AV300 spectrometer (300 MHz) in THF-d8 and is internally referenced to residual proton solvent signals (THF-d8: δ = 1.73 and 3.58 ppm). FAB mass spectrum was obtained with a VG-Quattro spectrometer in the positive-ion mode by using $CHCl_3$ as the solvent and m-nitrobenzyl alcohol (Sigma Aldrich) as the matrix.

Solvents used for spectroscopic measurements were of spectroscopic grade. UV/Vis spectra were measured with a Cary 100 spectrophotometer. Fluorescence measurements were performed on a Fluoromax-4 (HORIBA Scientific) spectrofluorimeter. FT-IR spectra of zinc prolinated porphyrin and porphyrin-ZnONP conjugate dispersed in nujol were recorded on a Perkin Elmer SpectrumOne spectrometer.

Microstructural and chemical analysis of samples (pure **ZnONP** and **ZnPL(-)-ZnONP**) was carried out by using a field emission scanning electron microscope (FE-SEM, SUPRA™ 35, Carl Zeiss SMT, Oberkochen, Germany) and energy dispersive microanalysis (EDX, INCAx-sight, Model: 7426, Oxford Instruments, Abingdon, Oxfordshire, UK).

CD spectra were performed on a JASCO J-600, equipped with a thermostated cell holder set at 298 K, and purged with ultra-pure nitrogen gas. CD measurements on chiral porphyrin films were carried out for different positions of the glass substrate (0, 90 and 180 degrees), obtaining similar spectra in all cases. This result ruled out significant contributions from linear dichroism effects.

Synthetic procedures. Porphyrin derivatives **H_2PL(-)** was prepared as previously reported.[6c]

Synthesis of ZnPL(-). To a stirred solution of porphyrin **H_2PL(-)** (100 mg, 0.131 mmol) dissolved in chloroform (15 mL), an excess of a saturated methanol solution of $Zn(AcO)_2$ was added. The progress of the reaction was monitored by UV-visible spectroscopy (Soret and Q visible bands changes). After 1 h, the metal insertion was complete and the solvent was removed *in vacuo* to give a cherry-purple solid, which was dissolved again in chloroform and washed with distilled water. The organic phase was dried on anhydrous Na_2SO_4 and then filtered. The desired complex was obtained as a pure purple powder after crystallization from chloroform/n-pentane (101 mg, 0.122 mmol; 93% yield). UV-Vis (THF): λ_{max} (ε, M^{-1} cm^{-1}) = 424 (451000), 556 (15500), 595 (5600) nm. ^{1}H NMR (300 MHz, THF-d_8): 8.83 (m, 8 H, β-pyrr), 8.21 (m, 4H, ArH), 8.19 (m, 6H, ArH), 7.76 (m, 3H,

ArH), 7.65 (m, 6H, ArH), 4.01 (m, 1 H, proline α-H), 3.91 (m, 2 H, proline δ- H), 2.36 (m, 2 H, proline β- H), 2.20 (m, 2 H, proline γ- H). FAB-MS (NBA), m/z: 818 $[M]^+$.

Preparation of porphyrin aggregates in hydroalcoholic solvent mixture. The formation of chiral porphyrin aggregates **ZnPL(-)-Agg** has been carried out in aqueous ethanol solutions (EtOH/H_2O 25/75 v/v; T= 298K) at 5μM concentration, using a "porphyrin first" protocol.[6c] First, a ZnPL(-) porphyrin stock solution in ethanol was prepared and filtered through a 0.2 μm Nylon® membrane (Hahnemüle Albet® Syringe Filters) prior to use. Check of the effective concentration was performed by UV/Vis spectroscopy (Soret band intensity of the porphyrin monomer; $\varepsilon = 4.51 \times 10^5\ M^{-1}cm^{-1}$). 63 μL of a millimolar stock solution of ZnPL(-) in ethanol (3.2×10^{-4} M) were added to the amount of ethanol (final volume of 1.0 mL) in an 8 mL glass vial. To this solution, 3.0 mL of water were then added, to give 4.0 ml of resulting solution with 25% v:v proportion and the final porphyrin concentration of 5μM. Porphyrin systems evolve within one week into chiral aggregates, as demonstrated by UV-Vis and CD Spectroscopy monitoring. The porphyrin stock solution should be used within two weeks from preparation, to ensure optimal reproducibility of the results.

Synthesis of ZnONP. ZnONP were prepared following the hydrothermal route reported in literature.[12] Briefly, the precursor solution, consisting of 5.3 g of $Zn(OAc)_2 \cdot 2H_2O$ dissolved in 80 mL of absolute ethanol, was poured in a Teflon Lined Hydrothermal Synthesis Autoclave Reactor that, in turn, has been kept at 120° C for 12 hours. After cooling down to room temperature, the formed nanoparticles were separated by centrifugation. Finally, they were rinsed in ethanol and annealed at 200 °C under argon flux for 2 hours.

Preparation of porphyrin-functionalized nanoparticles. Firstly, ZnONP were dispersed in Milli-Q grade D.I. water by ultrasonic bathing to obtain a uniform solution, without the presence of precipitate, then dried. 5 mg of dried nanoparticles were added to a solution of 3 mg of porphyrin derivative dissolved in 2 mL of toluene. The resulting mixture was kept under sonication for 3 hours. Functionalized nanoparticles were separated from unreacted porphyrins by successive centrifugations and dilutions in toluene, until the porphyrin Soret band was no longer detectable in the UV-Vis spectra of the supernatant liquid.

Preparation of solid films for fluorescence and circular dichroism studies. Films on glasses have been obtained by drop casting technique using samples in the proper solvent. Monomeric **ZnPL(-)** has been spotted using a 3.2×10^{-4} M solution of the title porphyrin in ethanol, while porphyrin

aggregates **ZnPL(-)-Agg** were deposited using a 5 µM porphyrin solution in EtOH:H_2O, 25:75 v:v mixture**.** Finally, hybrid nanoparticles were dispersed in toluene (6.5 mg/mL) and drop casted on a glass heated at 50°C to promote the solvent evaporation.

Quartz Microbalance. QMBs are mass transducers, where the decreasing of the resonance frequency is, in the small perturbation regime, linearly correlated to the increase of mass loading.[14]
The used QMBs were AT-cut quartzes oscillating in the thickness shear mode, at a fundamental frequency of approximately 20 MHz (KVG GmbH). The crystal diameter was 7.0 mm, with the gold electrodes diameter of 5.0 mm. Such quartzes have a theoretical mass sensitivity of about 4.8 Hz/ng, considering a minimum reliable frequency measurement of 1 Hz, it corresponds to a mass resolution of approximately 0.2 ng.[15]
ZnPL(-), ZnPL(-)-Agg, and **ZnPL(-)-ZnONP** were deposited onto both the QMB surfaces by drop casting the solution or suspension in the proper solvent. In case of porphyrin solution in ethanol, a 5 µl drop was casted onto the gold electrode; solvent evaporation was facilitated placing the sensor on a 50 °C hot plate. The procedure was repeated until a shift of 15 kHz was reached considering both sides of QMB. This oscillation frequency delta corresponds to *ca* 3 µg of material. In case of **ZnPL(-)-Agg**, the optimal conditions for the self-assembly process confines the concentration of **ZnPL(-)** to µM range, causing the deposition of 15 kHz of material a rather time consuming step. **ZnPL(-)-ZnONP** have been deposited starting from a high concentrated suspension in toluene (6.5 mg/mL, NB at this ratio, most of nanoparticles rapidly sediment). A single 5 µL drop is sufficient to produce a shift of 50 kHz in the QMB oscillation frequency. In this experiment 110 kHz of **ZnPL(-)-ZnONP** have been deposited considering both the faces of quartz, which is still largely in the linear response behaviour for 20 MHz QMB device. Considering the ZnO:porphyrin ratio evinced by EDX (Figure S2 and Table S1), this amount of hybrid nanoparticles bears *ca* 4 µg of porphyrin that is close to the quantity layered on the other two sensors.
Sensors were operated in an air-tight chamber with gas inlet and outlet. Each QMB was connected to an electronic oscillator circuit and the frequency of each oscillator was measured by an in-house designed electronics. Sensor responses were measured exposing the systems to 4%, 6% and 8% of saturated vapours of (R)- and (S)-limonene, (R)- and (S)-butan-2-ol and (-)- and (+)- alpha-pinene enantiomers diluted in a pure nitrogen gas carrier. Saturated vapours were obtained by bubbling pure nitrogen gas in the liquid sample kept at 25°C by a thermal bath.
At the reference temperature, the concentrations of saturated vapours of limonene, alpha-pinene and butan-2-ol result equal to 1980 ppm,[16a] 5822 ppm,[16b] and 24080 ppm[16c] respectively. The sensors responses to each concentration has been measured four times and a random order was used for each

sequence replica. Each measurement consisted in a gas exposure (5 minutes) followed by the exposure to the carrier gas (20 minutes). In the measurement sequence the enantiomers are alternately delivered at the same concentration to reduce time influence in the responses. Sensors signals were totally reversible. Flux and vapours dilutions were governed by a system of Mass Flow Controllers (MKS). The total flux at the inlet of the sensors cell has been always kept constant at 200 standard cubic centimetres per minute. The temperature of the whole system (liquid sample, gases, and sensors) was always kept at 25°C and the ambient humidity was maintained around 10% for the whole experiment.

3. RESULTS AND DISCUSSION

Preparation and characterization of porphyrin-based chiral systems. All the systems investigated in the present work are based on the inherently chiral porphyrin derivative **ZnPL(-)** which is readily achieved by metalation with $Zn(OAc)_2$ of the corresponding **H_2PL(-)** free base, previously studied by our group (see Chart 1).[6c] The appended (L)-proline unit confers both the amphiphilic and the chiral features to the porphyrin macrocycle, enabling the formation of chiral assemblies with specific geometry in hydroalcoholic mixture of proper composition. Indeed, the title porphyrin dissolved in ethanol is in monomeric form (Figure 1A, red line), but the controlled addition of a proper amount of water steers the self-aggregation process by hydrophobic effect. At micromolar concentrations, **ZnPL(-)** self-assembles in EtOH:H_2O 25:75 v:v, found as the optimal solvent composition for efficient and reproducible stereospecific evolution of these systems.

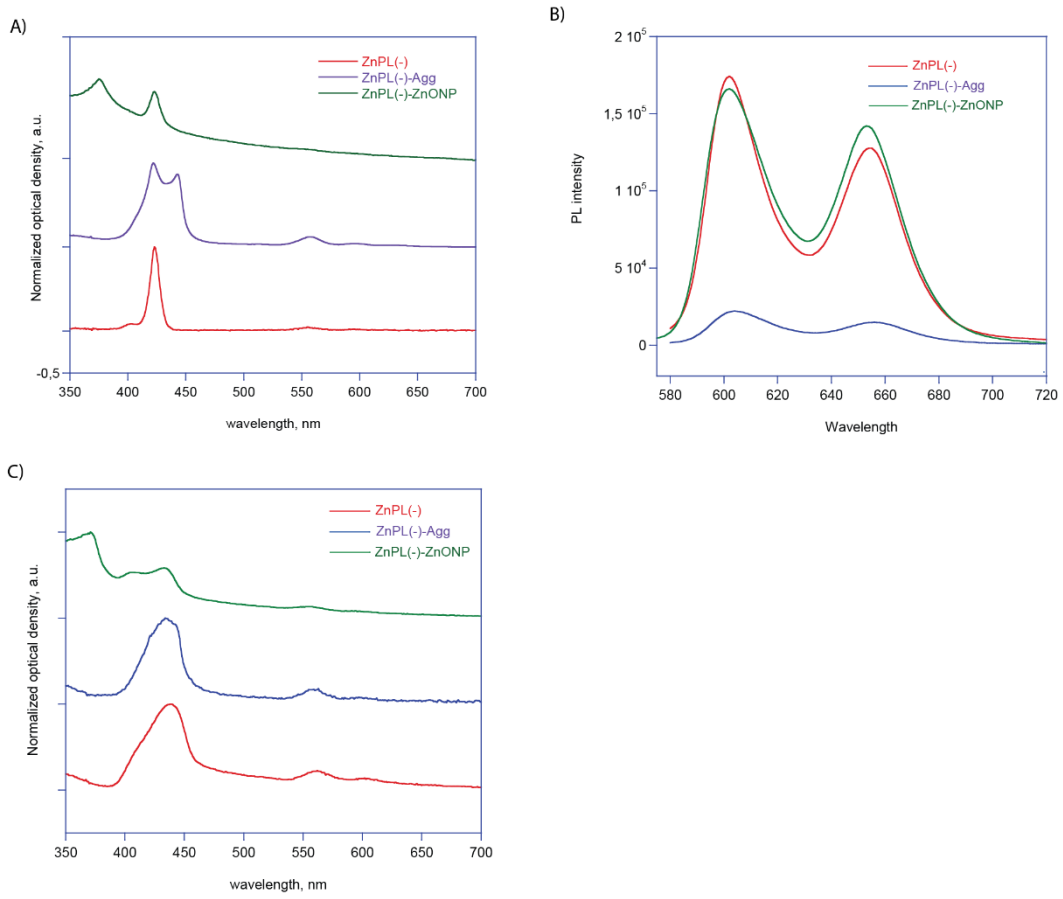

Figure 1. UV-Vis (A) and fluorescence spectra (emission spectra, λ_{ex}=424nm) (B) of the three systems investigated in solution. (C) UV-Vis spectra of the three systems dropped on glass slides.

The formation of **ZnPL(-)** chiral suprastructures (hereafter referred as **ZnPL(-)-Agg**) is clearly indicated by the typical UV-Vis spectral changes, showing the Soret band of the monomer evolving at equilibrium into a double peaked band of lower intensity (λ = 422 and 443 nm, respectively) (Figure 1A, blue line), indicative of the formation of ordered supramolecular structures with local J-type ($\boldsymbol{B_J}$) and H-type ($\boldsymbol{B_H}$) chiral axes.[17] Furthermore, fluorescence emission showed by these species in solution (600-700 nm region; λ_{exc} = 424 nm; Figure 1B blue line) is strongly quenched if compared to the **ZnPL(-)** monomers in ethanol (Figure 1B red line), corroborating the occurrence of aggregation steered by hydrophobic effect. The **ZnPL(-)-ZnONP** hybrid material was straightforwardly obtained by dispersing uncoated ZnO nanoparticles in a toluene solution of porphyrin under ultrasonic bath, to prevent the formation of clusters and maximize the area available for the grafting of porphyrins. To ensure a stable film onto nanoparticles, the residuals and unreacted porphyrin macrocycles are removed at the end of functionalization step by an appropriate washing procedure reported in the materials section.

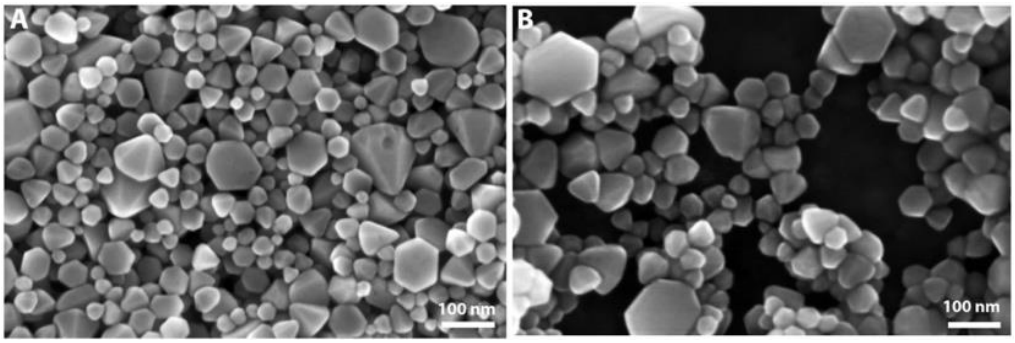

Figure 2. SEM images of (A) pure **ZnONP** and (B) **ZnPL(-)-ZnONP**.

The morphological characterization of decorated ZnO nanoparticles has been carried out by Scanning Electron Microscopy (SEM). As shown in Figure 2, nanoparticles appear as hexagonal pyramids, whose dimensions range from 10 to 120 nm (80% of sample lying in 25-65 nm interval, see SI, Figure S3). Predictably, the surface functionalization did not significantly affect neither the shape nor the size of nanostructures, as evidenced by the comparison between the uncoated and decorated nanoparticle samples (Figure 2A and 2B, respectively). Although a first direct evidence of porphyrins incorporation was given by the naked eye observation of changing in the colour of the nanoparticles (from white to pale red), Fourier Transform Infrared Spectroscopy (FT-IR) was used to verify the covalent functionalization. Indeed, IR spectra performed on **ZnPL(-)** and the **ZnPL(-)-ZnONP** conjugate in Nujol evidenced a broadened and shifted peak from 1682 cm^{-1} to 1672 cm^{-1} for the carboxylate group, corresponding to the porphyrin monomer and the hybrid material, respectively, indicative of covalent attachment via the proline residue to the ZnO surface (see SI, Figure S4). UV-Vis spectroscopy analysis performed in THF, chosen to avoid formation of clusters, showed that the conjugate displays the typical peak of ZnONP at 375 nm and a Soret band, centred at 424 nm, both clearly emerging from the large absorption tail of scattering baseline (Figure 1A, green line). The comparison of the spectral features of porphyrin monomers and hybrid conjugates showed only a slight broadening of the Soret band upon surface ligation, which still results at the same wavelength for the chromophore in the two cases.

Fluorescence measurements showed that the emission intensity of the ZnONP bound porphyrins did not significantly change with respect to **ZnPL(-)** (Figure 1B green and red line, respectively). This finding rules out the occurrence of strong aggregation phenomena between tetrapyrrolic macrocycles within the individual functionalized nanoparticles.

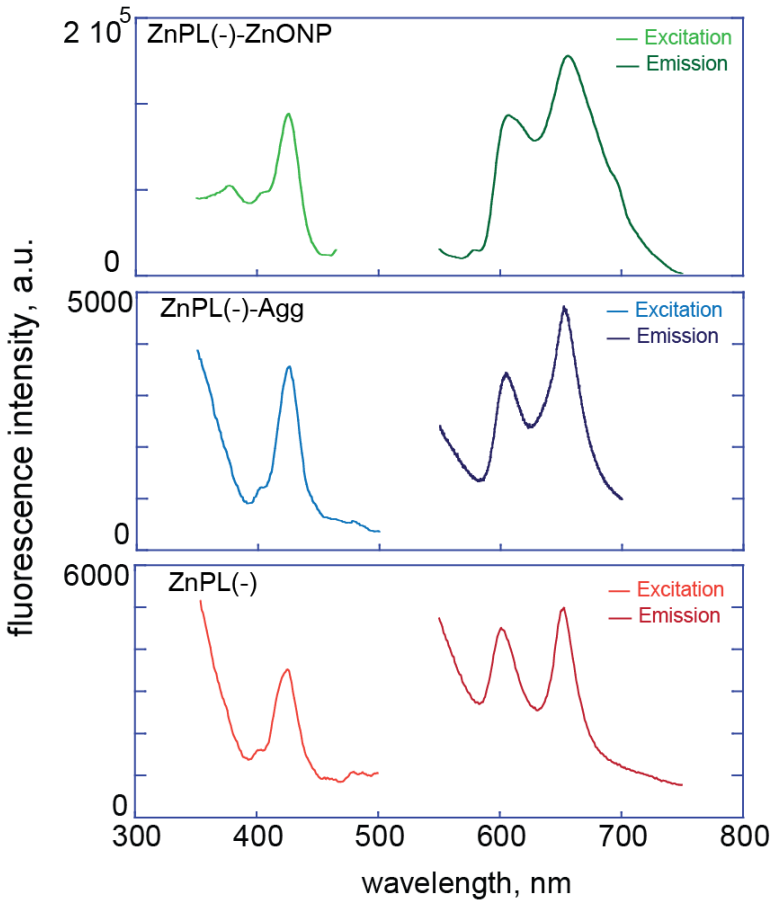

Figure 3. Fluorescence spectra of solid film made of **ZnPL(-)**,**ZnPL(-)-Agg** and **ZnPL(-)-ZnONP**. For excitation spectra λ_{em} = 606 nm, for emission spectra λ_{ex} = 424 nm.

Thin solid films on glass have been obtained by drop casting method from appropriate amounts of stock solutions of the three systems investigated. In the case of both the aggregates and drop casted monomers, UV-Vis spectra feature an evident broadening of B bands (Figure 1C, blue and red line respectively) and fluorescence emission spectra evidence a significant quenching of the emission intensities (Figure 3, A and B) indicating the formation of aggregated species. In the case of the layered hybrid ZnO-conjugates, Figure 1C (green line) shows a peculiar coupled feature of the absorption band, in close adherence to that observed for the aggregates in ethanolic aqueous solution (Figure 1A; blue trace). The corresponding excitation spectra (Figure 3C) reveals that two main contributions are responsible for the fluorescence emission of the conjugates: the first is due to porphyrin alike to **ZnPL(-)** and **ZnPL(-)-Agg** (peak at 427 nm) while the second one to the energy transfer from ZnO to the macrocycles (peak emerging at 375 nm).

Chiroptical properties of the investigated porphyrin-based systems. The possibility to achieve a chiral surface represents a crucial point for the stereoselectivity of the above described systems. Their

proper chiral organization both in solution and in solid state, has been investigated by means of Circular Dichroism Spectroscopy (CD) technique.

The ethanolic solution of **ZnPL(-)**, i.e. in monomeric form, is CD silent in the 350-500 nm region, indicating that the presence of the stereogenic centre of the appended proline does not appreciably induce chirality on the porphyrin macrocycles (data not shown).

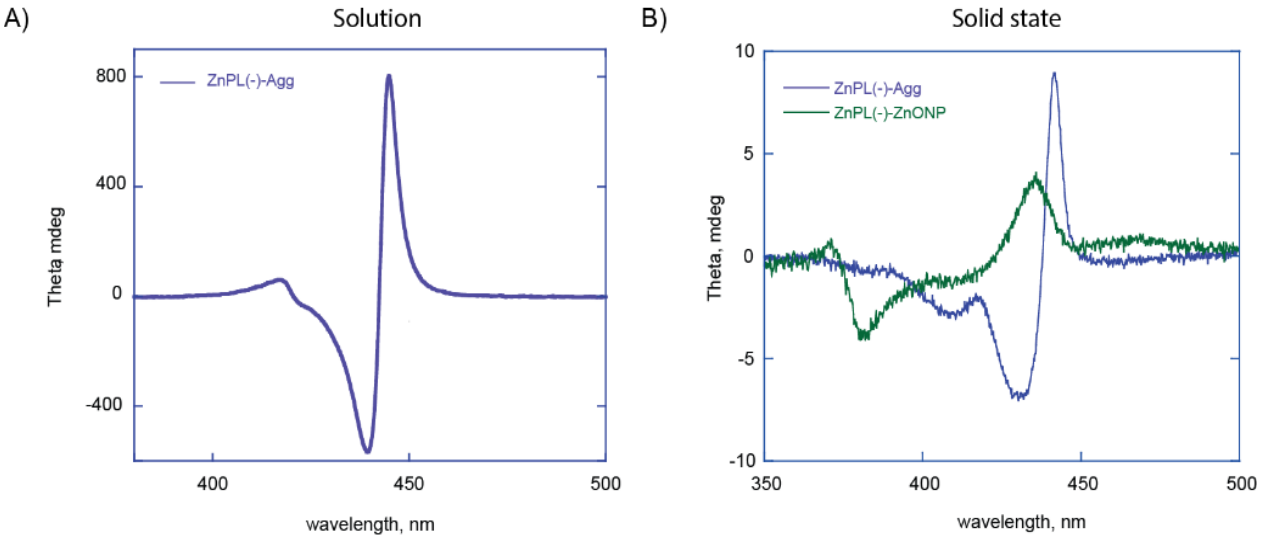

Figure 4. Circular dichroism spectra of (A) **ZnPL(-)-Agg** in ethanol/water (25:75, v/v) at 5 μM concentration; (B) **ZnPL(-)-Agg** deposited on glass slide from hydroalcoholic solvent mixture at 5 μM concentration (blue line) and **ZnPL(-)-ZnONP** deposited on glass slide from toluene at 6.5 mg/mL concentration (green line).

Remarkably, the supramolecular structures **ZnPL(-)-Agg** formed in EtOH:H_2O (25:75, v:v) show intense chiral features in the Soret B bend region (Figure 4A) as a result of the transmission of the chiral information stored on the L-proline group during the molecular recognition and growth of the suprastructures. A close inspection of the spectra reveals a +/-/-/+ sign, indicative of a mutual clockwise spatial arrangement (P configuration) for the $\boldsymbol{B_J}$ transition of the interacting porphyrin platforms, as excitonic theory suggests.[18]

In the case of the hybrid system **ZnPL(-)-ZnONP**, when the conjugates are well dispersed in solution (e.g. toluene or THF), CD spectra do not show significative signals emerging from the background noise (data not shown).

The above described materials have been deposited on glass slides. The inspection of corresponding CD spectra reveal that the solid film of **ZnPL(-)-Agg** retains the dichroic bands showed in solution

(Figure 4B, blue line), while the hybrid material shows multi-patterned coupled bands over the 350-500 nm range. Notably, besides the CD band on the region of porphyrin species (λ=446 nm), a dichroic band on the ZnO region (λ=375 nm) clearly appears, suggesting an effective chirality transfer via excitonic coupling from the tetrapyrrolic macrocycles to the ZnO surface (i.e. chirality induced effect.

Dichroic features emerge in solid films of porphyrins capped nanostructures, where presumably the establishing of favourable, asymmetric inter-particle coupling interactions between individual hybrid nanoparticles leads to new electronic states with chiroptical activity. Hence, it is reasonable to surmise that the interactions between the outer porphyrins of each nanostructure, besides promoting the solid films, also play a central role in the chiral transmission and amplification. It is to point out that chirality in inorganic nanostructures arising from inter-particle association is not unprecedented, being recently described in literature in various hybrid materials combining, among others, metal nanoclusters, semiconductor NPs or quantum dots (QDs) with chiral organic or biomolecules acting as templates.[19] Remarkably, it is worth to mention that, to the best of our knowledge, our result represents the first case of expression of chirality in porphyrin-functionalized ZnO nanomaterials.

Solid state stereoselectivity characterization. Stereoselective properties have been investigated measuring the sensitivity of Quartz Microbalances (QMBs) coated with layers of **ZnPL(-)**, **ZnPL(-)-Agg**, and **ZnPL(-)-ZnONP**. Sensing layers were obtained by drop casting technique following the same procedures used for the CD characterization.

Sensors were tested with vapours of enantiomer pairs: (R)- and (S)-limonene, (-)-alpha- and (+)-alpha-pinene, and (R)- and (S)-butan-2-ol. Enantiomers of each compound were alternately delivered to the sensors at three dilutions of saturated vapours in nitrogen gas (4%, 6% and 8% at T=298K). Measurements were made in quadruplicate and a random sequence of concentrations was applied in each replica.

Porphyrins, as molecules, offer a wide range of interactions for analyte binding, such as Van der Waals forces, hydrogen bond, π- π interactions and coordination to the metal atom;[20] and all these interactions are observed in porphyrins based sensors. In this case, additional interactions involving chiral sites are expected. Since the mass sensors are intrinsically nonselective respect to the nature of the interaction, it is clear that, to be observable, chiral interactions have to overcome all the other forces binding the analyte to the sensitive layer.

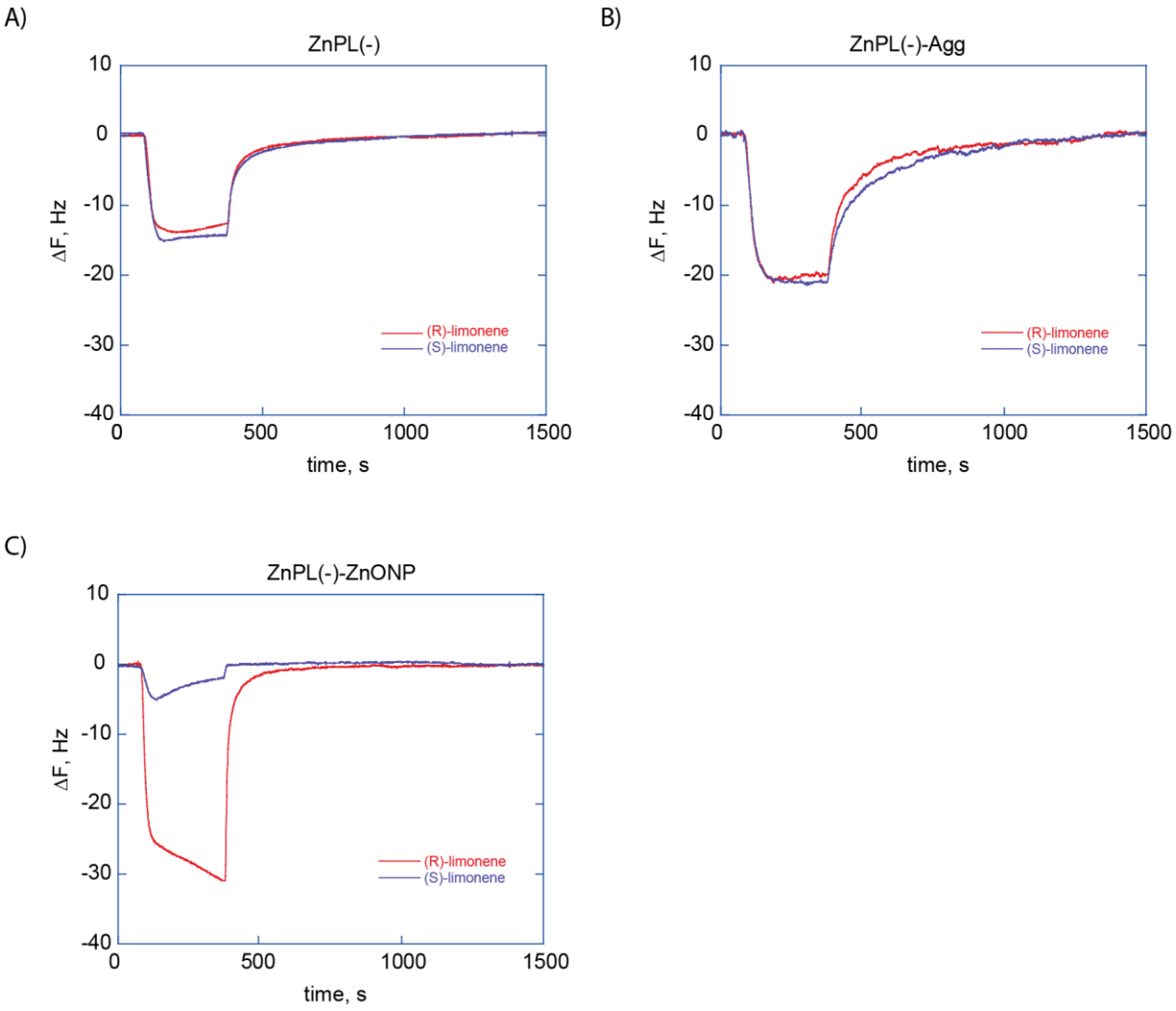

Figure 5. Dynamic of responses to 119 ppm of (R)- and (S)-limonene in the case of (A) **ZnPL(-), (**B) **ZnPL(-)-Agg** and (C) **ZnPL(-)-ZnONP** sensors.

Figure 5 shows the signal of the three sensors exposed to the same amount (6% of saturation pressure) of the enantiomers of limonene. The signals of sensors coated with **ZnPL(-)** monomers and aggregates (Figure 5A and 5B) are exactly the same considering (R)- and (S)-limonene responses. Furthermore, signals from both sensors quickly reach the plateau after the gas exposure. On the contrary, **ZnPL(-)-ZnONP** coated sensor shows a large asymmetry of the two signals, with the initial response to (R)-limonene almost 5 times larger than that to (S)-limonene. The dynamical behaviour of sensor signals suggests that the absorption processes involving hybrid and homogeneous materials are ruled by totally different mechanisms.

A more detailed representation of sensors behaviour is obtained studying the relationship between the concentration of the analytes and the largest difference of the QMB resonant frequency before and during the exposure to vapours. This quantity expresses the amount of absorbed molecules and

well represents the sensor response to the gas exposure. The behaviour of sensors response vs. concentration of alpha-pinene, butan-2-ol and limonene are shown in Figures S5, S6, and S7, respectively.

The three tested compounds are characterized by a different saturation pressure, as a consequence, the dilution of the saturated vapours results in different absolute fractional amounts. In this case it is convenient to consider the sensitivity of the sensors which is defined as the derivative of the sensor response respect to the concentration.[21]

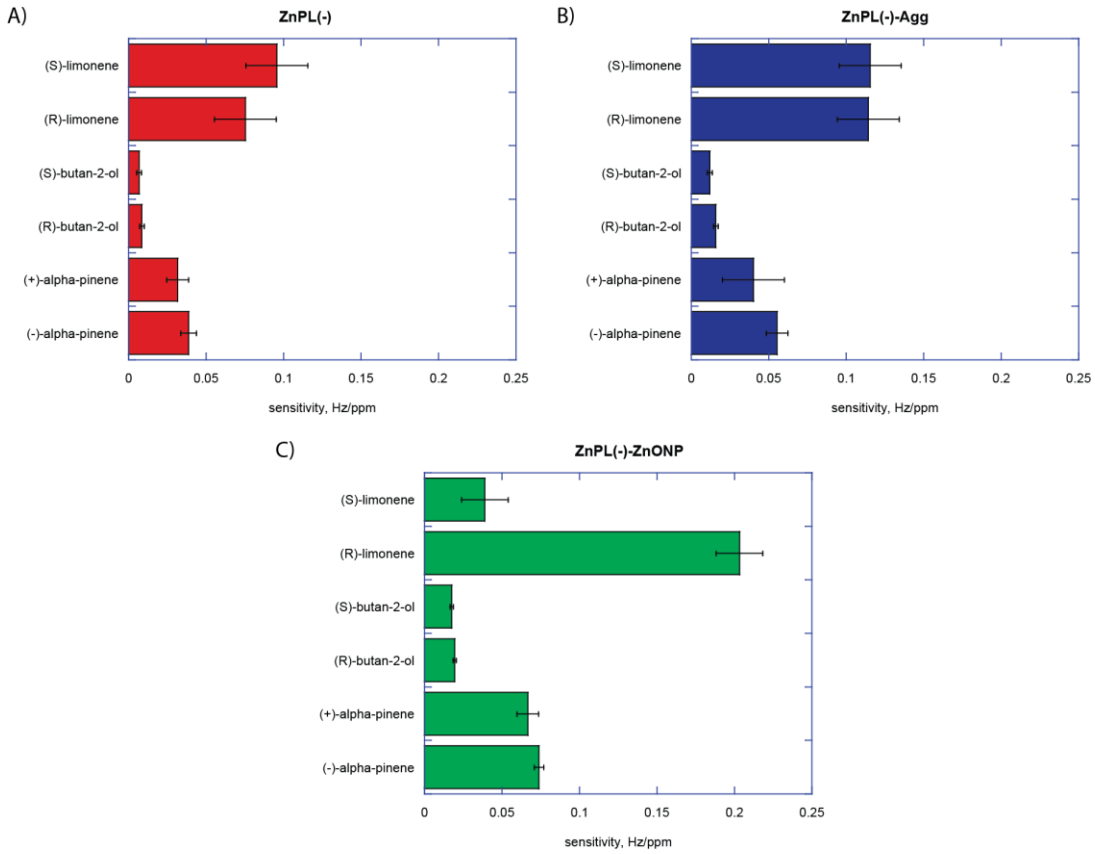

Figure 6: Sensitivity of (A) **ZnPL(-)**, (B) **ZnPL(-)-Agg** and (C) **ZnPL(-)-ZnONP** sensors to the enantiomers of the tested compounds. Data are fitted using a first-order polynomial function. Sensitivities are calculated as the first derivative of the fitting equation. Error bars report the 95% confidence bounds.

Figure 6 compares the sensitivity of each sensor respect to the enantiomers of the tested compounds. It is worth to note that all the three QMB sensors bear similar amount of sensing material, in case of hybrid **ZnPL(-)-ZnONP** the amount of porphyrin has been estimated by EDX analysis (Figure S2 and Table S1). As expected from Figure 5, the sensor coated with **ZnPL(-)-ZnONP** shows five times higher sensitivity towards (R)- enantiomer of limonene than (S)-limonene. Moreover, comparing the sensitivities of **ZnPL(-)-ZnONPs** to the ones obtained in case of **ZnPL(-)** and **ZnPL(-)-Agg**, the

chiral recognition ratio seems to be due to both an increase of (R)-limonene sensitivity and a decrease of (S)-limonene one.

ZnPL(-) monomers and aggregates do not show any statistical relevant difference among the enantiomers. In case of **ZnPL(-)-Agg**, chiroptical activity does not result in stereoselectivity of film. This outcome is not totally unexpected since the cationic counterparts, **MPL(+)**, was not able to discriminate chiral enantiomers too (see Figure S1).

As a general result, films made of ZnPL(-) as itself have a reduced sensitivities compared to the case of hybrid material and a lower reproducibility of responses. These two aspects are likely related to the reduced surface:volume ratio and to the difficulty to produce uniform film in case of anionic proline appended porphyrins. Except for the different sensitivity to (S)-limonene in case of **ZnPL(-)-ZnONP**, all of the sensors exhibit the highest sensitivity towards limonene vapours suggesting the diffusion of this analyte into the whole film during the adsorption phase. Actually limonene is relatively flat and can easily intercalate between the porphyrins composing the sensing layer. This outcome confirms that limonene is an optimal probe to investigate the stereoselective properties of porphyrin films. On the contrary, the reduced response to alpha-pinene could be due to the steric hindrance and rigidity of the molecule that make the diffusion of this molecule less probable (3D molecular models are reported in Figure S8). Sensitivities of three film to butan-2-ol and alpha pinene are strongly correlated in case of the three films and it is somehow expected considering that they bear the same sensing element (ZnPL(-)).

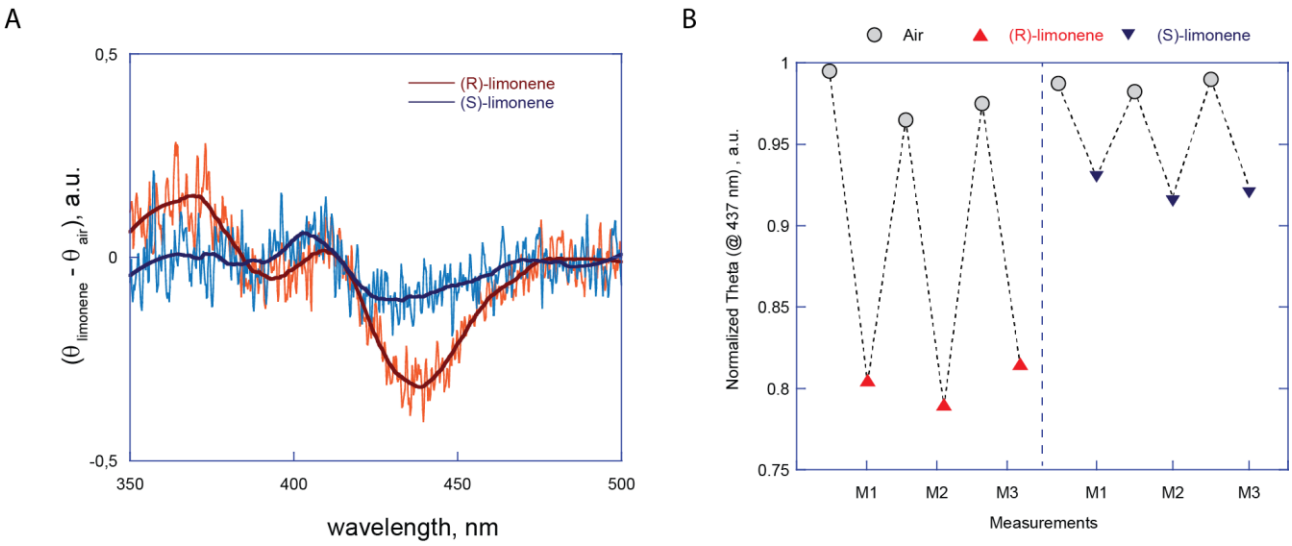

Figure 7. A) Differences of CD signal between air and saturated vapours of limonenes in the case of glasses coated with **ZnPL(-)-ZnONP** films. Data are normalized by the optical density measured in correspondence of the Soret peak, without considering the contribution of

scattering. B) shows repeatability and recovery of glass after the exposures to limonene enantiomers. CD signal at 437 nm are reported after the normalization of spectra.

An independent demonstration of stereorecognition of limonene vapours can be obtained measuring the CD signal of a solid layer of **ZnPL(-)-ZnONP** deposited on an optical glass slide when exposed to the vapours of the two limonene enantiomers. Figure 7A shows the variations of the CD signal obtained as the difference between the dichroic signal recorded after the exposure to saturated vapours and the reference one, acquired in ambient air conditions (25°C, RH ca 40%). The exposure to saturated vapours of (R)-limonene elicits a decrease of the CD signal respect to ambient air. Importantly, this effect has been found to be totally reversible and reproducible (Fig 7B) in accordance with the dynamic responses of QMB gas sensors. CD results corroborate the previous outcomes suggesting that limonene directly diffuses into the layer, favourably interacting with the large polarizable chiral surfaces and interrupting the electronic coupling among the tetrapyrrolic macrocycles, as indicated by the fact that the main variations occurs in the optical region of the aggregated porphyrin (band at 446 nm). This effect is almost negligible during the absorption of (S)-limonene even at saturated vapour concentrations. This result is in agreement with the QMB behaviour, and it indicates that the interaction with the (S)- counterpart is hindered by stereochemical mismatching.

4. CONCLUSIONS

This paper introduces a nanoscaled solid-state chiral system based on ZnO nanoparticles covalently conjugated to (L)-proline functionalized Zn porphyrin derivative (**ZnPL(-)-ZnONP**). The chiroptical properties of the studied systems were investigated by Circular Dichroism spectroscopy, both in solution and in solid state. These studies reveal the possibility to form chiral assemblies at supramolecular level by aggregating the hybrid systems during the film deposition step, as a consequence of solvent evaporation. Stereoselectivity was investigated studying the adsorption of some chiral analytes onto functionalized QMBs. Results show that **ZnPL(-)-ZnONP** conjugate displays a remarkable selectivity toward limonene enantiomers while other materials, although showing chiral properties, do not confer enantioselectivity to sensors. These results illustrate that chiroptical activity is a necessary but not sufficient condition for stereoselective solid state materials. Stereoselectivity requires an interaction between the analyte and chiral centres, which in turn must be reachable and not involved in other stronger bonds, and, as previously mentioned, the interaction via chiral sites must be in preference to non-specific adsorption mechanisms.

The peculiar morphology of the material made of porphyrins capped nanostructures confers the enantioselectivity within a large concentration range and very high chiral recognition ratio towards limonene enantiomers, which result as an optimal chiral probe due to the intercalation ability. Future studies, aimed at the optimization of film architectures, expanded toolbox of substituents on macrocycles periphery, and a wider selection of chiral functions, should result in significant improvements of the stereoselectivity of those hybrid systems towards a large series of chiral compounds.

We may foresee that these findings could be transferred also to liquid phase sensing, resulting in potential applications in important fields such as pharmaceutics, chemical, biotechnology and food industry.

SUPPORTING INFORMATION

A listing of the contents of each file supplied as Supporting Information should be included. For instructions on what should be included in the Supporting Information as well as how to prepare this material for publication, refer to the journal's Instructions for Authors. The Supporting Information is available free of charge on the ACS Publications website.

ACKNOWLEDGMENTS

This paper is dedicated to Professor Peter M. Maitlis in occasion of his 85th birthday.

This research has been partly funded by the University of Rome Tor Vergata, "Consolidate the Foundation (No. xcfed. Lunedì ve lo dico)" program, and INAIL, BRICS-ID12 project

We thank Giulia Monti for technical help and skill for TOC drawing.

REFERENCES

(1) Yoon, M.; Srirambalaji, R.; Kim K. Homochiral Metal–Organic Frameworks for Asymmetric Heterogeneous Catalysis *Chem. Rev*. **2012**, *112*, 1196-1231. b) Mallat, T.; Orglmeister, E.; Baiker, A. Asymmetric Catalysis at Chiral Metal Surfaces *Chem. Rev*. **2007**, *107*, 4863-4890. c) Wu, C-D; Hu, A.; Zhang, L.; Lin, W. A Homochiral Porous Metal−Organic Framework for Highly Enantioselective Heterogeneous Asymmetric Catalysis *J. Am. Chem. Soc*. **2005**, 127, 8940-8941

(2) a) Verbiest, T.; Kauranen, M.; Persoons, A. Second-order nonlinear optical properties of chiral thin films *J. Mat. Chem.* **1999**, *9*, 2005-2012. b) Fischer, P.; Hache, F. Nonlinear optical spectroscopy of chiral molecules *Chirality*, **2005**, *17*, 421-437. c) Valev, V. K.; Baumberg, J.J.;

De Clercq, B.; Braz, N.; Zheng, X.; Osley, E.J.; Vandendriessche, S.; Hojeij, M.; Blejean, C.; Mertens J. et al. Nonlinear superchiral meta-surfaces: Tuning chirality and disentangling non-reciprocity at the nanoscale *Adv. Mater.* **2014**, *26*, 4074-4081.

(3) a) Gellman, A. J. Chiral Surfaces: Accomplishments and Challenges *ACS Nano* **2010**, *4*, 5-10. b) Amabilino, D. B. Chiral nanoscale systems: preparation, structure, properties and function Chem. *Soc. Rev.* **2009**, *38*, 669-670. c) Wang, Y.; Xu, J.; Wang, Y. ; Chen, H. Emerging chirality in nanoscience *Chem. Soc. Rev.* **2013**, *42*, 2930-2962. d) Bradshaw, D. S.; Leeder, J. M.; Coles, M. M.; Andrews, D. L. Signatures of material and optical chirality: Origins and measures. *Chem. Phys Lett.* **2015**, *626*, 106-110.

(4) a) Ariga, K.; Richards, G. J.; Ishihara, S.; Izawa, H.; Hill, J. P. Intelligent Chiral Sensing Based on Supramolecular and Interfacial Concepts *Sensors* **2010**, *10*, 6796-6820. b) Moshe, H.; Vanbel, M.; Kolev Valev, V.; Verbiest, T.; Dressler, D.; Mastai, Y. Chiral thin films of metal oxide *Chem -Eur. J.* **2013**, *19*, 10295-10301. c) Labuta, J.; Hill, J.P.; Ishihara, S.; Hanykova, L.; Ariga, K. Chiral Sensing by Nonchiral Tetrapyrroles *Acc. Chem. Res.* **2015**, *48*, 521-529. d) Huang, H.; Bian, G.; Zong, H.; Wang, Y.; Yang, S.; Yue, H.; Song, L.; Fan, H. Chiral Sensor for Enantiodiscrimination of Varied Acids. *Org. Lett.* **2016**, *18*, 2524-2527. e) Torsi, L.; Farinola, G. M.; Marinelli, F.; Tanese, M. C.; Omar, O. H.; Valli, L.; Babudri, F.; Palmisano, F.; Zambonin, P. G.; Naso, F. A sensitivity-enhanced field-effect chiral sensor. *Nat. Mat.* **2008**, *7*, 412-417. f) Bodenhöfer, K.; Hierlemann, A.; Seemann, J.; Gauglitz, G.; Koppenhoefer, B.; Göpel, W. Chiral discrimination using piezoelectric and optical gas sensors *Nature* **1997**, *387*, 577-580

(5) a) Monti, D. Recent Advancements in Chiral Porphyrin Self-Assembly. In Synthesis and Modification of Porphyrinoids – Topics in Heterocyclic Chemistry, Vol. 33 (Ed. R. Paolesse), Springer, 2014, pp 231-291. b) Borovkov, V. Supramolecular Chirality in Porphyrin Chemistry *Symmetry* **2014**, *6*, 256-294. c) Vela, S.; Berrocal, J. A.; Atienza, C.; Meijer, E. W.; Martin, N. Mesoscopic helical architectures via self-assembly of porphyrin-based discotic systems *Chem. Commun.* **2017**, *53*, 4084-4087. d) Oliveras-Gonzalez, C.; Di Meo, F.; Gonzalez-Campo, A.; Beljonne, D.; Norman, P.; Simon-Sorbed, M.; Linares, M.; Amabilino, D. B. Bottom-Up Hierarchical Self-Assembly of Chiral Porphyrins through Coordination and Hydrogen Bond J. *Am. Chem. Soc.* **2015**, *137*, 15795-15808. e) Mabesoone, M.F.J.; Markvoort, A.J.; Banno, M.; Yamaguchi, T.; Helmich, F.; Naito, Y.; Yashima, E.; Palmans, A. R.A.; Meijer E. W. Competing

Interactions in Hierarchical Porphyrin Self-Assembly Introduce Robustness in Pathway Complexity *J. Am. Chem. Soc*. **2018**, *140*, 7810−7819.

(6) a) Monti, D.; Venanzi, M.; Mancini, G.; Di Natale, C.; Paolesse, R. Supramolecular chirality control by solvent changes. Solvodichroic effect on chiral porphyrin aggregation *Chem. Commun.* **2005**, 2471-2473. b) Monti, D. ; Venanzi, M.; Stefanelli, M.; Sorrenti, A.; Mancini, G.; Di Natale, C.; Paolesse, R. Chiral Amplification of Chiral Porphyrin Derivatives by Templated Heteroaggregation *J. Am. Chem. Soc*. **2007**, *129*, 6688 – 6689. c) Monti, D.; De Rossi, M.; Sorrenti, A.; Laguzzi, G.; Gatto, E.; Stefanelli, M.; Venanzi, M.; Luvidi, L.; Mancini, G.; Paolesse, R. Supramolecular Chirality in Solvent-Promoted Aggregation of Amphiphilic Porphyrin Derivatives: Kinetic Studies and Comparison between Solution Behavior and Solid-State Morphology by AFM Topography *Chem. Eur. J.* **2010**, *16*, 860-870.

(7) Bidleman, T. F.; Jantunen, L. M.; Kurt-Karakus, P. B.; Wong, F. Chiral persistent organic pollutants as tracers of atmospheric sources and fate: review and prospects for investigating climate change influences *Atmospheric Pollution Research* **2012**, *3*, 371-382

(8) Manoli, K.; Magliulo, M.; Torsi, L., Chiral sensor devices for differentiation of enantiomers *Top Curr Chem* **2013**, *341*, 133–176

(9) Paolesse, R.; Monti, D.; La Monica, L.; Venanzi, M.; Froiio, A., Nardis, S.; Di Natale, C. ; Martinelli, E. ; D'Amico, A. Preparation and Self-assembly of Chiral Porphyrin Diads on the Gold Electrodes of Quartz Crystal Microbalances: A Novel Potential Approach to the Development of Enantioselective Chemical Sensors *Chem. Eur. J.* **2002**, *8*, 2476-2483

(10) Monti, D.; Stefanelli, M; Raggio, M; Colozza, N.; Venanzi, M.; Lettieri, R. ; Luvidi, L.; Laguzzi, G.; Bonacchi, S.; Weber, D.; Prodi, L.; Di Natale, C.; Paolesse, R.; *J. Porphyrins Phthalocyanines* **2011**, *15*, 1209-1219

(11) Schmidt-Mende, L., J. L. MacManus-Driscoll, *Mater. Today* **2007**, *10*, 40-48. b) Djurišić, A. B.; Chen, X.; Leung, Y. H.; and Ng, A. M. C.; *J. Mater. Chem.* **2012**, *22*, 6526-6535.

(12) a) Saarenpaä, H.; Sariola-Leikas, E.; Pyymaki Perros, A.; Kontio, J. M.; Efimov, A.; Hayashi, H.; Lipsanen, H.; Imahori, H.; Lemmetyinen, H.; Tkachenko, N. V.; *J. Phys. Chem. C* **2012**, *116*,

2336-2343. b) Tu, W., Lei, J., Wang, P., & Ju, H. Photoelectrochemistry of Free-Base-Porphyrin-Functionalized Zinc Oxide Nanoparticles and Their Applications in Biosensing. *Chemistry–A European Journal* **2011**, *17*(34), 9440-9447.c) Hayashi, H., Lightcap, I. V., Tsujimoto, M., Takano, M., Umeyama, T., Kamat, P. V., & Imahori, H. Electron transfer cascade by organic/inorganic ternary composites of porphyrin, zinc oxide nanoparticles, and reduced graphene oxide on a tin oxide electrode that exhibits efficient photocurrent generation. *Journal of the American Chemical Society* **2011**, *133*(20), 7684-7687.d) Aly, S. M., Eita, M., Khan, J. I., Alarousu, E., & Mohammed, O. F. Remarkable fluorescence enhancement versus complex formation of cationic porphyrins on the surface of ZnO nanoparticles. *The Journal of Physical Chemistry C* **2014**, *118*(23), 12154-12161.e) Düring, J., & Gröhn, F. ZnO nanorods assembled with different porphyrins–size-tunable hybrid particles. *RSC Advances* **2017**, *7*(6), 3321-3330. f) Sivalingam, Y., Martinelli, E., Catini, A., Magna, G., Pomarico, G., Basoli, F., ... & Di Natale, C. Gas-sensitive photoconductivity of porphyrin-functionalized ZnO nanorods. *The Journal of Physical Chemistry C* **2012**, *116*(16), 9151-9157. g) Magna, G., Sivalingam, Y., Martinelli, E., Pomarico, G., Basoli, F., Paolesse, R., & Di Natale, C. The influence of film morphology and illumination conditions on the sensitivity of porphyrins-coated ZnO nanorods. *Analytica chimica acta* **2014**, *810*, 86-93.

13) Magna, G., Zor, S. D., Catini, A., Capuano, R., Basoli, F., Martinelli, E., ... & Di Natale, C. Surface arrangement dependent selectivity of porphyrins gas sensors. *Sensors and Actuators B: Chemical* **2017**, *251*, 524-532.

14) Ballantine Jr, D. S., White, R. M., Martin, S. J., Ricco, A. J., Zellers, E. T., Frye, G. C., & Wohltjen, H. In Acoustic wave sensors: theory, design and physico-chemical applications, Elsevier, **1996**

15) D'Amico, A.; Di Natale, C.; A contribution on some basic definitions of sensors properties *IEEE Sens. J.* **2001**, *1*, 183-190.

16) a) Dıaz, M. E., Guetachew, T., Landy, P., Jose, J., & Voilley, A. Experimental and estimated saturated vapour pressures of aroma compounds. *Fluid Phase Equilibria* **1999**, *157*(2), 257-270.b) Hawkinds, J. E.; Armstrong, G. T.; Physical and Thermodynamic Properties of Terpenes.1 III. The Vapor Pressures of α-Pinene and β-Pinene *J. Am. Chem. Soc.* **1954**, *76*, 3756-3759. c) Nasirzadeh, K., Zimin, D., Neueder, R., & Kunz, W.; Vapor-pressure measurements of liquid solutions at different temperatures: Apparatus for use over an extended temperature range and some new data. *Journal of Chemical & Engineering Data* **2004**, *49*(3), 607-612.

17) Ohno, O., Kaizu, Y., & Kobayashi, H.; J-aggregate formation of a water-soluble porphyrin in acidic aqueous media. *The Journal of chemical physics* **1993**, *99*(5), 4128-4139.

18) a) Berova N and Nakanishi K. In Circular Dichroism. Principles and Applications, 2nd ed., Berova N, Nakanishi K and Woody RW., Ed., John Wiley & Sons: New York, **2000**; pp 337. b) Pescitelli, G., Gabriel, S., Wang, Y., Fleischhauer, J., Woody, R. W., & Berova, N.; Theoretical Analysis of the porphyrin− porphyrin exciton interaction in circular dichroism spectra of dimeric tetraarylporphyrins. *Journal of the American Chemical Society* **2003**, *125*(25), 7613-7628.

19) a) Kumar, J., Thomas, K. G., & Liz-Marzán, L. M.; Nanoscale chirality in metal and semiconductor nanoparticles. *Chemical Communications*, *52*(85), 12555-12569.b) Duan, Y., Han, L., Zhang, J., Asahina, S., Huang, Z., Shi, L., Wang, B., Cao, Y.; Yao, Y.; Ma, L.; Wang, C.; Dukor, R.K.; Sun, L., Jiang, C.; Tang, Z.; Nafie, L.A.; Che, S. Optically Active Nanostructured ZnO Films. *Angewandte Chemie International Edition* **2015**, *54*(50), 15170-15175. c) Ma, W., Xu, L., de Moura, A.F., Wu, X., Kuang, H., Xu, C., Kotov, N.A. Chiral inorganic nanostructures. *Chem. Rev.* **2017**, *117*, 8041−8093.

20) Di Natale, C., Monti, D. and Paolesse, R. Chemical sensitivity of porphyrin assemblies *Materials today* **2010**, *13*(7-8) 46-52.

21) D'Amico, Arnaldo, and Corrado Di Natale. "A contribution on some basic definitions of sensors properties." *IEEE Sensors Journal* **2001**, *1*(3), 183-190.